A hybrid continuum-kinetic framework to model ionic liquid ion source emission

IEPC-2022-233

Presented at the 37th International Electric Propulsion Conference
Massachusetts Institute of Technology, Cambridge, MA, USA
June 19-23, 2022

Amin Taziny[1], Wai Hong Ronald Chan[2], Iain D. Boyd[3]
University of Colorado, Boulder, CO, 80303

A hybrid continuum-kinetic framework to model electrospray thrusters based on ionic liquid ion source emission is presented. The framework couples two computational domains that span multiple scales: the emitter tip at the site of ion evaporation and downstream where ions are advected, denoted as the Extraction Region and Plume Region, respectively. In the Extraction Region, a multigrid electrohydrodynamic model solves the Laplace and Stokes equations via finite element methods, where an iterative routine enforces surface charge evolution and stress balance at the meniscus. In the Plume Region, a combined particle-in-cell/direct simulation Monte Carlo approach treats far-field ion transport. A novel treatment of directionally-dependent boundary conditions is developed to enforce the coupled field emission equations, and the predicted thrust is validated against experimental measurement. The framework seeks to elucidate life-limiting mechanisms of electrospray thrusters by relating performance parameters across the wide range of spatial scales.

I. Nomenclature

$\mathbf{E}_l$	=	bulk fluid electric field vector
$\mathbf{E}_v$	=	vacuum electric field vector
$\mathbf{E}_0$	=	applied electric field
h_c	=	Planck constant
$h_{\gamma_{lv}}$	=	characteristic length scale of element on Γ_{lv}
I	=	emission current
$\mathbf{j}$	=	current density vector
k_b	=	Boltzmann constant
K	=	electric conductivity
m	=	ion mass
$\hat{\mathbf{n}}$	=	unit vector normal to interface
p	=	pressure
q	=	elementary charge
r^*	=	characteristic length scale at emission tip
$\hat{\mathbf{t}}$	=	unit vector tangent to interface
T	=	temperature
$\mathbf{v}$	=	bulk fluid velocity vector
Γ_{lv}	=	intersection between liquid and vacuum domain in Extraction Region
γ	=	surface tension

[1]Ph.D. Student, Ann and H.J. Smead Aerospace Engineering Sciences, Amin.Taziny@colorado.edu
[2]Post-Doctoral Fellow, Ann and H.J. Smead Aerospace Engineering Sciences, WaiHongRonald.Chan@colorado.edu
[3]H. T. Sears Memorial Professor, Ann and H.J. Smead Aerospace Engineering Sciences, Iain.Boyd@colorado.edu

ΔG = solvation energy of EMI-BF_4 ions
ϵ_0 = vacuum permittivity
ϵ = relative permittivity
μ = dynamic viscosity of bulk fluid
ν = test function defined in Sobolev space $H^1(\Omega)$
ρ = density of bulk fluid
σ = free surface charge density
τ_l = viscous stress tensor
τ_e = electrostatic Maxwell stress tensor
ϕ_l = bulk fluid electric potential
ϕ_v = vacuum electric potential
Ω_l = computational bulk liquid domain in Extraction Region
Ω_v = computational vacuum domain in Extraction Region
Ω_p = computational vacuum domain in Plume Region

II. Introduction

Electrospray thrusters are a promising means of propulsion for miniaturized spacecraft and have been explored since the mid-20th century [1–3]. These systems operate by applying strong electric fields to conductive fluids, generating thrust from extracted droplets and ionic species. A subset of electrosprays use ionic liquids, or room temperature molten salts, as propellant due to their low volatility and ease in achieving a more efficient purely ionic emission [4]. These ionic liquid ion sources (ILISs) are often passively fed through capillary or porous-based emitters, where a meniscus forms at the liquid-vacuum interface. Exposure to strong potential gradients deforms the meniscus into a characteristic conical shape known as a Taylor cone, a result of the balance between electric traction of the induced field and surface tension. Unlike their liquid-metal counterparts, ILISs can operate at lower applied voltages at room temperature, allowing for wider mission applicability. Additionally, ILISs have been shown to emit beams of positive and negative polarities [5], allowing for bipolar operation where space charge accumulation can be mitigated. However, the low thrust-per-emitter of ILISs necessitates grid multiplexing for broader-scale mission applicability outside of fine attitude control. This is further obfuscated by life-limiting mechanisms of single-emitter systems, which are not well characterized to this day. The purpose of this study is to develop a high-fidelity computational framework capable of predicting basic ILIS operation.

The primary mechanism that leads to thruster failure is overspraying at the site of emission, leading to larger half-angles of emission that impinge on the extraction and acceleration grids, resulting in the pooling of propellant [6]. Thuppul et al. [6] also demonstrate that overspray impingement, as well as other failure mechanisms, such as electron backstreaming, are strongly dependent on choice of geometry. As such, lifetime models that capture plume characteristics on the grid must consider the influence of upstream characteristics beyond the site of emission. To accomplish this, a wide range of spatial scales must be resolved. For example, within passively fed porous configurations, it has been shown that beam composition is significantly altered by pore size, where characteristic length scales can range from 1 to 2 orders of magnitude higher than those at the site of emission [7]. Proper treatment of the electrohydrodynamics (EHD) at the liquid meniscus must be considered as well. Although ideal conductor models can demonstrate the evolution of meniscus shape [8], they cannot account for species emission without considering tangential charge transport.

Several works of interest have previously investigated the EHD of an ionic liquid meniscus. Higuera [9] developed a model of an ILIS operating in purely ionic emission using an order-of-magnitude formulation. As such, it was postulated that space charge effects in this regime are negligible and that the ion evaporation current is governed by the conductivity of the propellant. Coffman et al. [10] expanded upon this using the ionic liquid l-ethyl-3-methyl imidazolium tetrafluoroborate (EMI-BF4), adding consideration of viscous and Ohmic heating as well as a liquid feed system to emulate emitter conditions. Petro et al. [11] were first to explore ion emission modeling across multiple scales, combining EHD fluid and n-body particle models to predict performance. In this study, we present a multiscale framework that bridges ion emission from an EHD model of an ionic liquid meniscus to kinetic analysis, where downstream transport in the plume is studied. Thus, a direct connection can be made between upstream conditions at the emitter and plume characteristics that may contribute to electrospray lifetime mechanisms. Standard finite element methods are used to model fluid flow and electrostatic fields, while novel multigrid and boundary formulations are developed to enforce conditions at the liquid-vacuum interface, inspired by similar cone-jet routines [12]. A

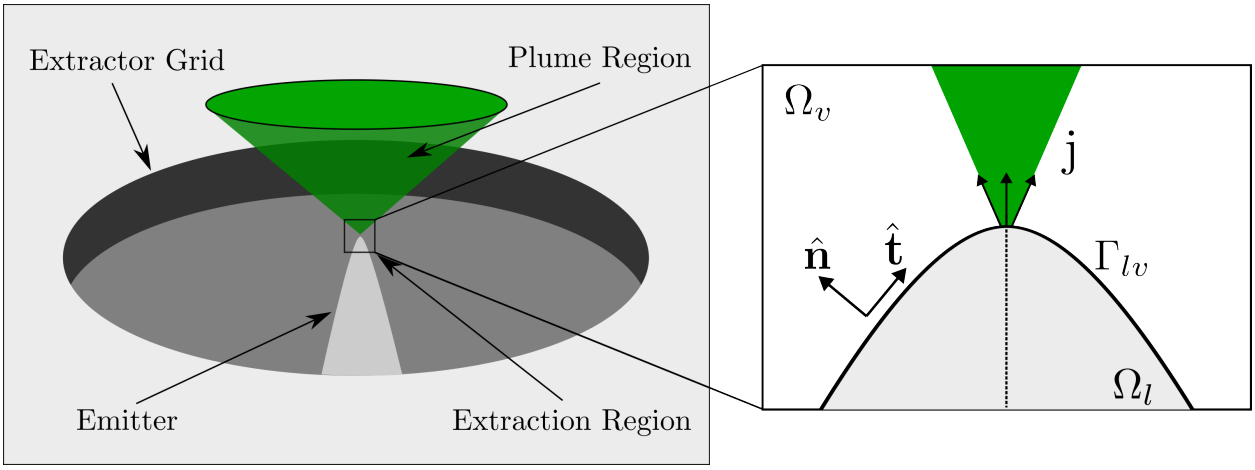

Fig. 1 Schematic of the multiscale domains of interest within an ILIS

particle-in-cell/direct simulation Monte Carlo (PIC/DSMC) solver [13] is used to treat species interaction in the plume. This novel framework aims to compute germane ILIS characteristics, including plume divergence, thrust, and emitter current. The framework also aims to illustrate the relationship between these parameters and the configuration geometry across spatial scales.

The paper is structured as follows. Section III introduces the methodology implemented in this work, including a description of how the domain is partitioned, the governing equations used within each regime, and the numerical routines of the solvers. Verification and results are discussed in Section IV, where a test case is presented to enforce a unique boundary condition required for ion emission, the parameters of simulation cases are described, electric potentials of the coupled domains are shown, Stokesian flow and ion emission at the emitter tip are discussed, and the simulation output of thrust and current is compared with experimental measurement. Conclusions are presented in Section V.

III. Methodology

A. Domain Description

The continuum-kinetic framework partitions a physical domain within an ILIS into two two-dimensional computation domains that span two orders of magnitude, as shown in Fig. 1. The first includes the EHD meniscus at the emitter tip where field emission occurs, denoted as the Extraction Region. The latter represents the domain where the extracted species are advected downstream the extractor grid, denoted the Plume region. The Extraction Region is further decomposed into a vacuum and bulk liquid domain, Ω_v and Ω_l, respectively, where Γ_{lv} denotes the intersection between them. The governing equations within this regime are presented in Section III.B, and its numerical implementation is presented in Section III.C. Kinetic treatment within the Plume Region is more established, thus this study largely focuses on model development within the Extraction Region. A brief description of the PIC/DSMC routines implemented in the Plume Region is presented in Section III.D.

B. Governing Equations – Extraction Region

Within the bulk liquid domain, momentum and mass conservation are enforced using the Stokes equations,

$$\mu \nabla^2 \mathbf{v} - \nabla p = 0, \tag{1}$$

$$\nabla \cdot \mathbf{v} = 0, \tag{2}$$

where μ is the fluid viscosity, $\mathbf{v}$ is the the bulk fluid velocity, and p is the pressure. Inertial forces are neglected as viscous effects have been shown to dominate and is generally unaffected by the mass flux of evaporated species [9]. Uniform electrical conductivity is assumed and an Ohmic conduction model is used for the current density. Using charge conservation, it can be shown that electric potential within the bulk fluid satisfies Laplace's equation,

$$\nabla \cdot \mathbf{j} = 0 \tag{3}$$

$$\mathbf{j} = K\mathbf{E}_l, \tag{4}$$

$$\nabla^2 \phi_l = 0, \tag{5}$$

where $\mathbf{j}$ is the current density, K is the electrical conductivity, $\mathbf{E_l}$ is the electric field in the bulk fluid, and ϕ_l is the potential in the bulk fluid. Laplace's equation is also considered within the vacuum domain,

$$\nabla^2 \phi_v = 0, \tag{6}$$

where ϕ_v is the electric potential in the vacuum domain. At the liquid-vacuum interface, the continuity of electric potentials between materials is enforced. Discontinuities in the electric field normal to the interface are accounted for in the free surface charge density,

$$\phi_l = \phi_v, \tag{7}$$

$$(-\nabla \phi_v + \epsilon \nabla \phi_l) \cdot \hat{\mathbf{n}} = \frac{\sigma}{\epsilon_0}, \tag{8}$$

where $\hat{\mathbf{n}}$ is the unit vector normal to the interface, σ is the free surface charge density, ϵ is the relative permittivity, and ϵ_0 is the vacuum permittivity. Steady-state surface charge transport is also considered,

$$\mathbf{v} \cdot \nabla \sigma = \sigma \hat{\mathbf{n}} \cdot \nabla \mathbf{v} \cdot \hat{\mathbf{n}} + K\mathbf{E}_l \cdot \hat{\mathbf{n}} - \mathbf{j} \cdot \hat{\mathbf{n}}. \tag{9}$$

Equation (9) states that the charge advected by the fluid flow is balanced by surface strain, the charge conducted to the surface, and the charge lost due to ion evaporation. Field emission of ions is described by the kinetic law initially proposed by Iribarne and Thomson [14],

$$\mathbf{j} \cdot \hat{\mathbf{n}} = \frac{k_b T}{h_c} \sigma \exp\left(\frac{-1}{k_b T} \left[\Delta G - \sqrt{\frac{\nabla \phi_v \cdot \hat{\mathbf{n}}}{4\pi\epsilon_0 / q^3}} \right] \right), \tag{10}$$

where k_b is the Boltzmann constant, h_c is the Planck constant, T is the temperature, q is the elementary charge and ΔG is the solvation energy of the ions.

Additionally, force balance between the applied electric traction, viscous stresses, and surface tension is enforced at Γ_{lv},

$$\hat{\mathbf{t}} \cdot (\tau_l - \tau_e) \cdot \hat{\mathbf{n}} = 0, \tag{11}$$

$$\hat{\mathbf{n}} \cdot (\tau_l - \tau_e) \cdot \hat{\mathbf{n}} = -\gamma \nabla \cdot \hat{\mathbf{n}}, \tag{12}$$

where $\hat{\mathbf{t}}$ is the unit vector tangent to the interface, τ_l is the viscous stress tensor, τ_e is the electrostatic Maxwell stress tensor, and γ is the surface tension. The normal and tangential projections of the Maxwell stress tensor on the interface are provided by Saville [15],

$$\hat{\mathbf{t}} \cdot \tau_e \cdot \hat{\mathbf{n}} = -\sigma \nabla \phi_v \cdot \hat{\mathbf{t}}, \tag{13}$$

$$\hat{\mathbf{n}} \cdot \tau_e \cdot \hat{\mathbf{n}} = \frac{1}{2}\epsilon_0 \left((\nabla \phi_v \cdot \hat{\mathbf{n}})^2 - \epsilon (\nabla \phi_l \cdot \hat{\mathbf{n}})^2 \right) + \frac{1}{2}\epsilon_0 \left((\epsilon - 1)(\nabla \phi_v \cdot \hat{\mathbf{t}})^2 \right). \tag{14}$$

C. Model Description – Extraction Region

Equations (1)–(10) and Eqs. (12)–(14) are solved using finite element methods within the Distributed and Unified Numerics Environment (DUNE), an open-source, modular C++ library for solving partial differential equations via grid-based methods [16–18]. Propellant material properties are chosen to emulate the ionic liquid EMI-BF_4 and an applied potential gradient, $\nabla\phi = \mathbf{E_0}$, is enforced as a far-field condition within the Extraction Region. The framework begins by solving for the electric potential within the bulk fluid and vacuum domains (Eqs. (5)-(6)), under the electrostatic boundary conditions defined in Eqs. (7)–(8). Instead of iterating between domains, a global routine is implemented that solves both potentials simultaneously while enforcing continuity and the surface charge jump conditions at the interface. To accomplish this, the weak formulation of Laplace's equation is found by multiplying Eqs. (5)-(6) with a test function ν from their corresponding Sobolev spaces. This is shown using the bilinear form,

$$a(\phi, v) := \int_\Omega \langle \nabla\phi, \nabla v \rangle \, d\Omega, \tag{15}$$

where $\langle \cdot, \cdot \rangle$ denotes the inner product. The boundary value problem is then discretized using the Symmetric Interior Penalty Galerkin (SIPG) method [19], where the discrete residual of the problem

$$r\left((\phi_l, \phi_v), (v_l, v_v)\right) = \int_{\Omega_l} \nabla\phi_l \cdot \nabla v_l \, d\Omega_l + \int_{\Omega_v} \nabla\phi_v \cdot \nabla v_v \, d\Omega_v \tag{16a}$$

$$- \int_{\Gamma_{lv}} \{\langle \nabla\phi, \hat{\mathbf{n}} \rangle\} [\![v]\!] \, d\Gamma_{lv} - \int_{\Gamma_{lv}} \{\langle \nabla v, \hat{\mathbf{n}} \rangle\} [\![\phi]\!] \, d\Gamma_{lv} \tag{16b}$$

$$+ \kappa \sum_{\gamma_{lv} \in \Gamma_{lv}} \frac{1}{h_{\gamma_{lv}}} \int_{\gamma_{lv}} [\![\phi]\!][\![v]\!] \, d\Gamma_{lv} \tag{16c}$$

$$- \int_{\Gamma_{lv}} [\![\langle \nabla\phi, \hat{\mathbf{n}} \rangle]\!][\![v]\!] \, d\Gamma_{lv}, \tag{16d}$$

is minimized. Note the jump and average of values across the interface are defined as $[\![\phi]\!] := \phi_l - \phi_v$ and $\{\phi\} := \frac{1}{2}(\phi_l + \phi_v)$, respectively. Equation (16a) represents the volumetric residual within each subdomain. Equations (16b)–(16c) couple the subdomains at the interface, penalizing jumps across the boundary and enforcing potential continuity. Similarly, Eq. (16d) allows a Neumann jump condition to be prescribed at the interface to account for surface charge. This requires a slight reformulation of Eq. (8),

$$[\![\langle \nabla\phi^i, \hat{\mathbf{n}} \rangle]\!] = \frac{\sigma^i}{\epsilon_0} - (\epsilon - 1) \, \nabla\phi_l^{i-1} \cdot \hat{\mathbf{n}}, \tag{17}$$

where ϕ_l^{i-1} denotes the liquid electric potential from the previous iteration.

Electric potentials from the multidomain Poisson model are used to solve for the total current density, the sum of current from Ohmic conduction (Eq. (4)) and that convected at the surface (Eq. (9)). Ion evaporation at the interface assumes that normal fluid flow is nonzero, otherwise mass would not be conserved. For this relation, we look to

$$\mathbf{v} \cdot \hat{\mathbf{n}} = \frac{\mathbf{j} \cdot \hat{\mathbf{n}}}{\rho(q/m)}, \tag{18}$$

where ρ is the density of the fluid and m is the mass of the solvated species [20]. Equations (11) and (18) are then used to specify the boundary conditions at the interface for the Stokes routine. The Stokes problem (Eqs. (1)–(2)) is also handled using standard finite element methods. Due to the mass continuity constraint, the corresponding weak formulation is a saddle-point problem and is handled using canonical Taylor-Hood elements. Unique treatment of the boundary conditions mentioned above is required, as a Dirichlet condition (Eq. (18)) is enforced normal to the interface, while a Neumann condition (Eq. (13)) is enforced in the tangential direction. This is further discussed in Section IV. Solutions to the Stokes equations are used to find the next iteration of the free surface charge density, and the iterative process repeats until a sufficient residual is met. This iterative process is shown in Fig. 2. As the shape of the meniscus is preimposed, it is salient to note that any residual within Eq. (12) denotes a non-equilibrium balance in normal forces, requiring iteration of the intersection curvature. This is deferred to future work.

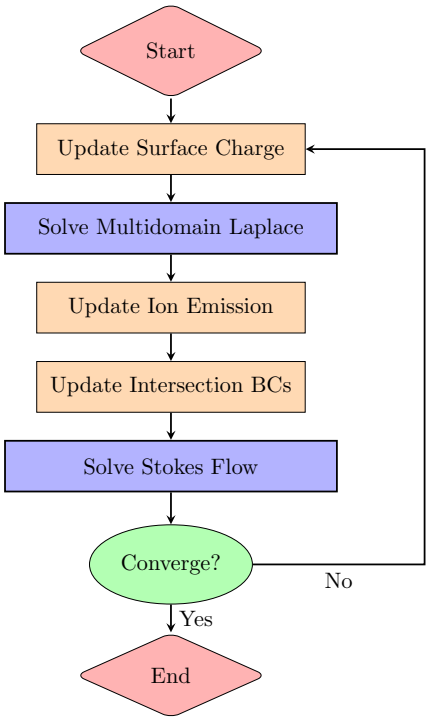

Fig. 2 Algorithm to numerically solve for ion emission from the EHD meniscus within the Extraction Region

D. Model Description - Plume Region

The plume domain, Ω_p, utilizes the DSMC method [21] to model the motion and collisions of the emitted species in combination with standard PIC methods to capture acceleration of charged due to the applied and self-generated electric fields. For this study, emitted species are limited to positive ions and no electrons are considered.

IV. Verification and Results

A. Dual normal-Dirichlet, tangential-Neumann Boundary Condition

A unique consideration of the boundary conditions (11)-(18) is required for the Stokes problem, and a test case is conducted to demonstrate its implementation. The simultaneous constraints of a normal-projected velocity and tangent-projected viscous stress tensor at the interface require a dimensionally-dependent enforcement of both a Dirichlet and Neumann boundary condition. Physically, this corresponds to fluid flow normal to the meniscus due to ion emission, whereas viscous stresses act on the component of fluid moving tangentially to the free surface. While the Neumann condition naturally arises in the weak formulation of the Stokes problem, the Dirichlet condition requires weak enforcement using an added coercivity term. This term depends on an arbitrarily large penalty factor, α, which requires calibration such that the ratio of the boundary conditions is approximately unity; otherwise, the conditions are not enforced equally. As this penalty factor is problem dependent, a simple, qualitative test case is conducted to determine its value for viscous length-scales, shown in Fig. 3. A box of side-length unity is chosen, where zero-Neumann conditions are enforced at the top and bottom boundaries, a no-slip and no-penetration condition at the left boundary, and a dual normal-Dirichlet tangential-Neumann—both of magnitude unity—at the right boundary. The tangent vector direction is mirrored about the horizontal center. Using the fluid properties of EMI-BF_4, Fig. 3 demonstrates quasi-equal enforcement of the directionally-dependent boundary conditions.

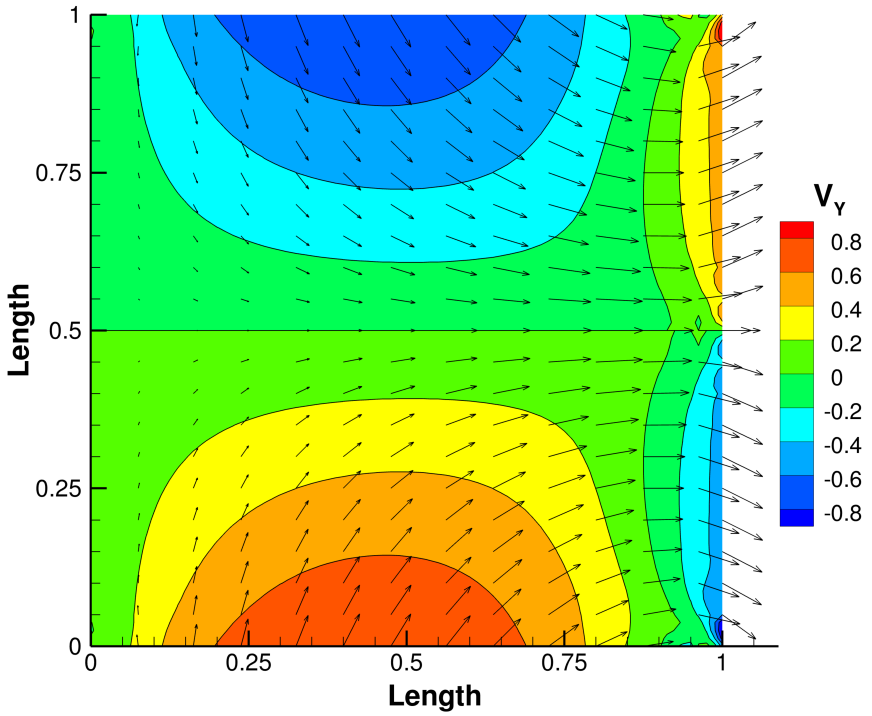

Fig. 3 Test case demonstrating balance of dual normal-Dirichlet tangential-Neumann boundary condition at right outlet

B. Simulation Parameters

Continuum and kinetic simulations are conducted based on operational conditions of porous ILIS data measured by Natisin et al. [5]. An applied voltage of -1562 V is chosen as the comparison case that the DSMC/PIC simulations are compared against. Mapping of ion emission of the EHD meniscus model to the kinetic routine is not directly calculated. Experimental current values are used as input conditions into the kinetic routine via single cell injection at the emitter tip. The applied electric field condition within the EHD model is then calibrated so that the integrated surface emission at the meniscus tip is of approximate order to the experimental current. Direct mapping of field emission from the EHD model within the Extraction Region to the kinetic model in the Plume Region is deferred to future work. A computational domain axial length of 0.1 μm and width of 0.1 μm is chosen for the Extraction Region, to emulate similar length scales of effective flow paths within porous ILIS emitters. Meshes of the liquid and vacuum subdomains in the Extraction Region are shown in Fig.4. A Taylor Cone angle of 49.29° is chosen for the emitter cone with a tip radius of 10 nm. Mesh elements at the emitter tip are refined in both subdomains to better resolve ion emission in this region. The computational domain of the Plume Region spans a radial distance of 500 μm and 1000 μm axially.

C. Electric Potentials

Electric potential distributions within the liquid and vacuum subdomains of the Extraction Region are presented in Fig. 5. A relatively linear progression is seen in the axial direction of both domains, with continuity between electric potentials at the interface. This is expected due to the prescribed boundary conditions of a fixed potential difference at the far-field. Thus, larger deviations from this linear profile due to the field of emitted ions and surface charge distribution at the interface are not seen, suggesting smaller induced fields of these parameters relative to the applied field. This is potentially due to the preimposed meniscus shape, where the balance of normal stresses across the interface from the electric field traction and surface tension is not enforced. Electric potential within the Plume Region is presented in Fig. 6. Qualitative agreement of the potential contours at the Extraction Region boundary is seen with the macroscopic potentials observed within the kinetic domain.

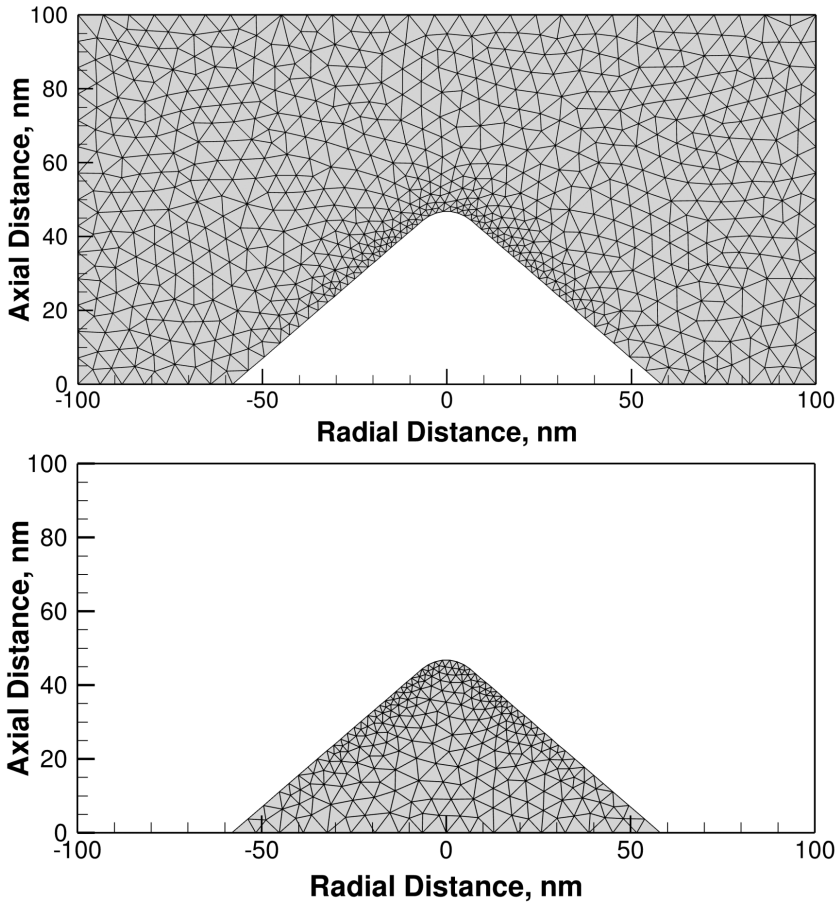

Fig. 4 Computational meshes of the liquid and vacuum subdomains within the Extraction Region

D. Stokesian Flow and Ion Emission

Axial velocity contours within the liquid subdomain of the Extraction Region are presented in Fig.7. Flow velocity of an ionic liquid meniscus operating in a purely ionic regime is known to scale with

$$v \sim \frac{I}{\pi\rho(q/m)(r^*)^2}, \tag{19}$$

where r^* is the characteristic length scale at the emitter tip and I is the emission current [20]. The Reynolds number scaling is then shown to be

$$Re \sim \frac{I}{\pi\mu(q/m)r^*} \sim 10^{-2}. \tag{20}$$

Using the single-emitter current for the -1562V operational case ($I \approx 10^{-6}$A) in [5] and the fluid properties of EMI-BF_4 ($\mu \approx 10^{-2}$ Pa· s, $q/m \approx 10^6$ C/kg), the Reynolds number is shown to be significantly less than unity and thus Stokesian flow is present. As mentioned in Section III.C, ion emission is only possible within a steady-state configuration if the normal fluid velocity at the intersection is nonzero. Field emission at the emitter tip is represented by arrows in the top-right plot of Fig. 7. Using Eq. (18), it can be shown that the velocity at the emission tip is of approximate order to the emission velocity in the operational case, though it is important to note that the applied electric field, $\mathbf{E_0}$, is adjusted in the Extraction Region to achieve this agreement.

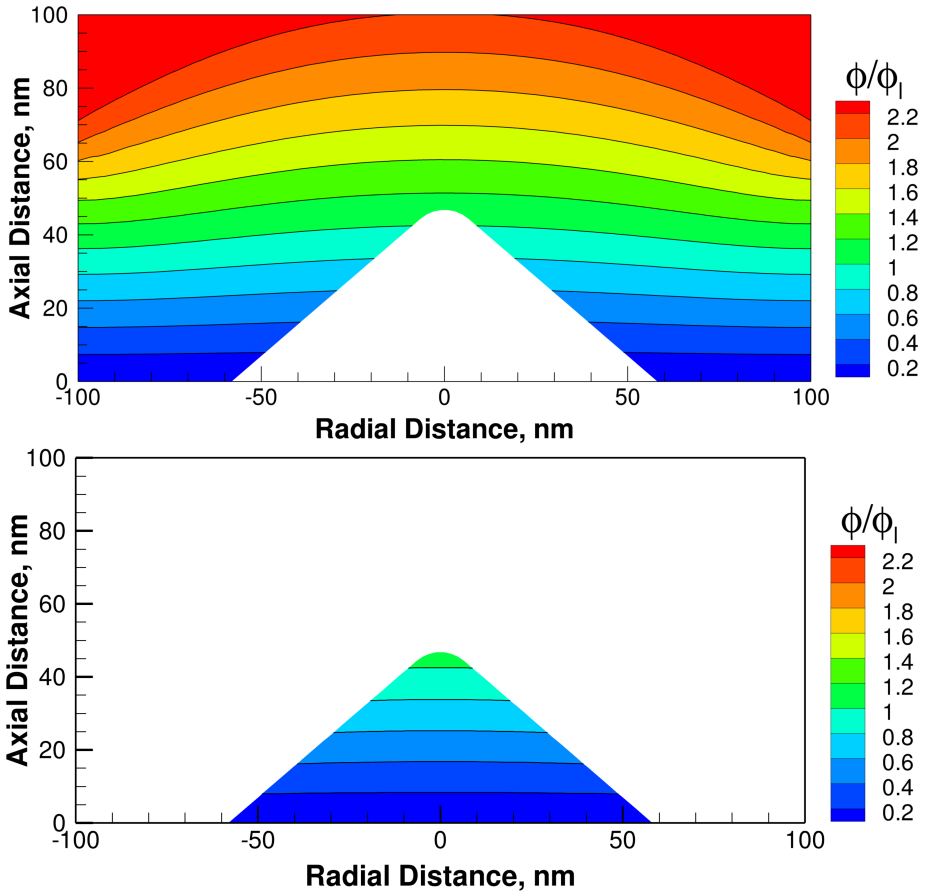

Fig. 5 Electric potentials within the liquid and vacuum subdomains of the Extraction Region, normalized by the liquid potential at the emitter tip

E. Comparison with Experiment

Using a range of operating extractor voltages, several DSMC/PIC simulations are conducted to determine the number density and axial velocity of positive EMI ions. Number flux and momentum are then calculated. These values are integrated about the plane 1000 μm away from the emitter base to determine emitter current and thrust. Current and thrust are then scaled to represent a multiplexed array of 576 emitters, the number used in experimentation by Natisin et al. [5]. Comparison of the emission current and thrust between experimental measurements and kinetic simulations across extractor voltages is presented in Fig. 8. Agreement is shown between the experimental data and simulation output, validating the DSMC/PIC model implemented in the Plume Region for downstream ion transport.

V. Conclusion

Electrospray thrusters have demonstrated high specific impulse and thrust-to-power ratios and, when multiplexed, generate thrust capabilities suitable for select micropropulsion systems, with the potential to expand to larger spacecraft. However, electrosprays have not yet been deployed at scale due to their limited lifetimes. The predominant life-limiting mechanism is believed to be pooling of propellant at the extractor and accelerator grids, which can occur for a multitude of reasons. For example, small changes in geometry and operating conditions, such as modifying grid aperture radius and spacing, can improve thruster lifetime by 200-400%. As such, it is clear a key component in increasing electrospray lifetime is optimization of geometry and operating conditions. Numerical modeling is an efficient means of accomplishing this as testing multiple geometric and operational parameters is streamlined within a computational environment. For a model to accomplish this, it must account for the underlying relationship between the physics that govern different regimes. These regimes often vary in scales of magnitude, necessitating multiscale consideration in its

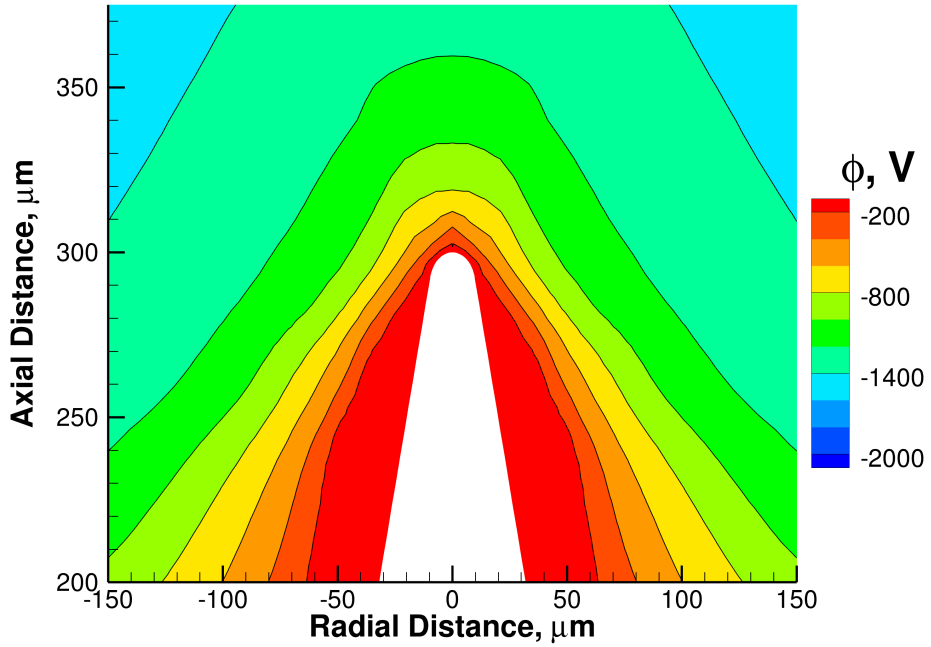

Fig. 6 Electric potentials within the Plume Region, where the emitter structure is equipotential

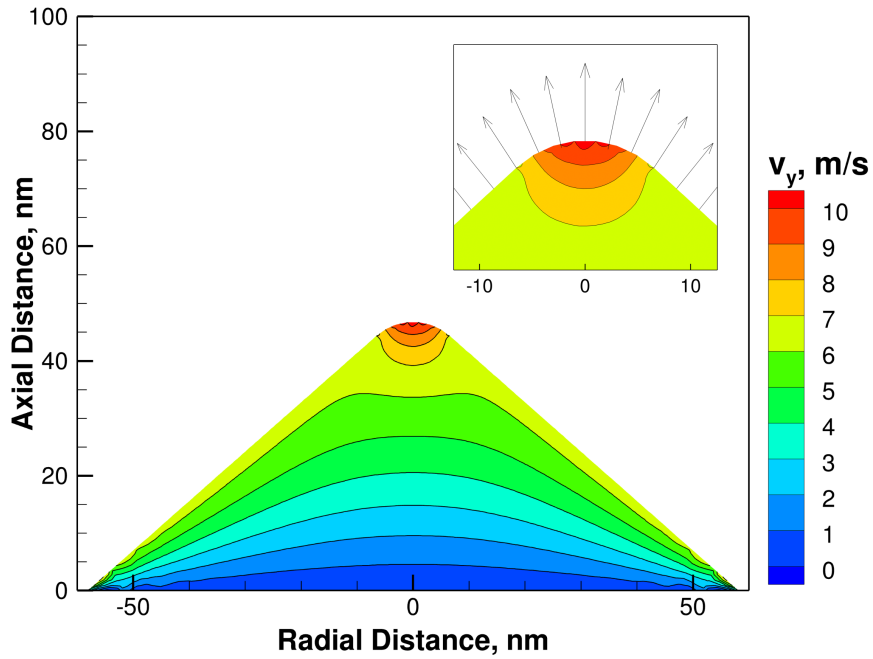

Fig. 7 Axial velocity distribution in the bulk fluid, with ion emission at the emitter tip shown in the inset

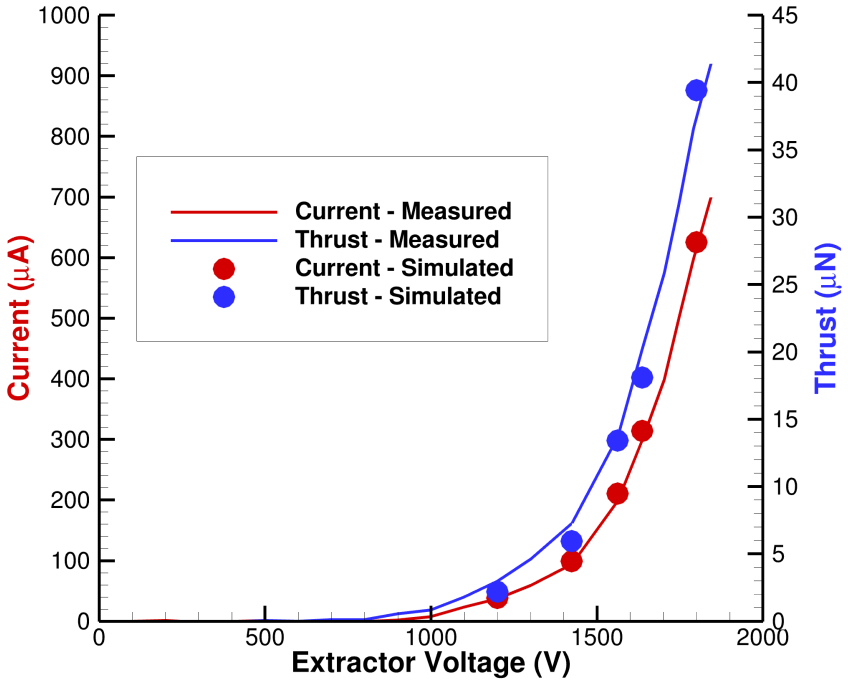

Fig. 8 Comparison of measured emission current and thrust by Natisin et al. [5] vs. simulated results by the DSMC/PIC solver across various extractor voltages

calculations.

This study aimed to take the first step towards this, modeling two characteristic scales within an ILIS pivotal in life-limiting mechanisms. We demonstrated the capability of using operational conditions of one scale—applied voltage by the extractor grid—and accurately modeling a dependent performance parameter—ion emission at the emitter tip—at a different scale. To implement this, a high-fidelity model was developed for each domain and numerical methods germane to each system were used to solve the governing equations. The EHD of the conductive meniscus was handled using finite elements across materials, where an iterative algorithm and novel means of enforcing directionally-dependent boundary conditions was used to solve for ion emission. After emission, continuum methods are no longer suitable in describing ion behavior and kinetic methods were used. A PIC/DSMC solver handled ion transport and induced fields by the accelerating charges. This multiphase routine was then validated using experimental measurements performed under similar operating conditions. Continued development of the model will seek to find equilibrium meniscus shapes within the Extraction Region, and better map parameters as they cross between domains. The simulations presented in this work demonstrate the potential of using numerical modeling to increase electrospray lifetime, allowing wider applicability within spacecraft missions.

Acknowledgments

The authors would like to thank computational resources from the Alpine Research Computing services of the University of Colorado. This work is supported by the Air Force Office of Scientific Research, Grant #FA9550-21-1-0045.

References

[1] Dole, M., Mack, L. L., Hines, R. L., Mobley, R. C., Ferguson, L. D., and Alice, M. B., "Molecular beams of macroions," *The Journal of chemical physics*, Vol. 49, No. 5, 1968, pp. 2240–2249.

[2] O'Reilly, D., Herdrich, G., and Kavanagh, D. F., "Electric propulsion methods for small satellites: A review," *Aerospace*, Vol. 8,

No. 1, 2021, p. 22.

[3] Krejci, D., and Lozano, P., "Space propulsion technology for small spacecraft," *Proceedings of the IEEE*, Vol. 106, No. 3, 2018, pp. 362–378.

[4] Lozano, P., and Martinez-Sanchez, M., "Ionic liquid ion sources: characterization of externally wetted emitters," *Journal of colloid and interface science*, Vol. 282, No. 2, 2005, pp. 415–421.

[5] Natisin, M., Zamora, H., McGehee, W., Arnold, N., Holley, Z., Holmes, M., and Eckhardt, D., "Fabrication and characterization of a fully conventionally machined, high-performance porous-media electrospray thruster," *Journal of Micromechanics and Microengineering*, Vol. 30, No. 11, 2020, p. 115021.

[6] Thuppul, A., Wright, P. L., Collins, A. L., Ziemer, J. K., and Wirz, R. E., "Lifetime considerations for electrospray thrusters," *Aerospace*, Vol. 7, No. 8, 2020, p. 108.

[7] Courtney, D. G., and Shea, H., "Influences of porous reservoir Laplace pressure on emissions from passively fed ionic liquid electrospray sources," *Applied Physics Letters*, Vol. 107, No. 10, 2015, p. 103504.

[8] Betelú, S., Fontelos, M., Kindelán, U., and Vantzos, O., "Singularities on charged viscous droplets," *Physics of Fluids*, Vol. 18, No. 5, 2006, p. 051706.

[9] Higuera, F., "Model of the meniscus of an ionic-liquid ion source," *Physical Review E*, Vol. 77, No. 2, 2008, p. 026308.

[10] Coffman, C., Martínez-Sánchez, M., Higuera, F., and Lozano, P. C., "Structure of the menisci of leaky dielectric liquids during electrically-assisted evaporation of ions," *Applied Physics Letters*, Vol. 109, No. 23, 2016, p. 231602.

[11] Petro, E. M., Gallud, X., Hampl, S. K., Schroeder, M., Geiger, C., and Lozano, P. C., "Multiscale modeling of electrospray ion emission," *Journal of Applied Physics*, Vol. 131, No. 19, 2022, p. 193301.

[12] Gamero-Castaño, M., and Magnani, M., "Numerical simulation of electrospraying in the cone-jet mode," *Journal of Fluid Mechanics*, Vol. 859, 2019, pp. 247–267.

[13] Cai, C., *Theoretical and numerical studies of plume flows in vacuum chambers*, University of Michigan, 2005.

[14] Iribarne, J., and Thomson, B., "On the evaporation of small ions from charged droplets," *The Journal of Chemical Physics*, Vol. 64, No. 6, 1976, p. 2287.

[15] Saville, D., "Electrohydrodynamics: the Taylor-Melcher leaky dielectric model," *Annual review of fluid mechanics*, Vol. 29, No. 1, 1997, pp. 27–64.

[16] Blatt, M., Burchardt, A., Dedner, A., Engwer, C., Fahlke, J., Flemisch, B., Gersbacher, C., Gräser, C., Gruber, F., Grüninger, C., Kempf, D., Klöfkorn, R., Malkmus, T., Müthing, S., Nolte, M., Piatkowski, M., and Sander, O., "The Distributed and Unified Numerics Environment, Version 2.4," *Archive of Numerical Software*, Vol. 4, No. 100, 2016, pp. 13–29. https://doi.org/10.11588/ans.2016.100.26526, URL http://dx.doi.org/10.11588/ans.2016.100.26526.

[17] Bastian, P., Heimann, F., and Marnach, S., "Generic implementation of finite element methods in the Distributed and Unified Numerics Environment (DUNE)," *Kybernetika*, Vol. 46, 2010, pp. 294–315.

[18] Dedner, A., Girke, S., Klöfkorn, R., and Malkmus, T., "The DUNE-FEM-DG module," *Archive of Numerical Software*, Vol. 5, No. 1, 2017, pp. 21–61. https://doi.org/10.11588/ans.2017.1.28602, URL http://journals.ub.uni-heidelberg.de/index.php/ans/article/view/28602.

[19] Douglas, J., and Dupont, T., "Interior penalty procedures for elliptic and parabolic Galerkin methods," *Computing methods in applied sciences*, Springer, 1976, pp. 207–216.

[20] Coffman, C. S., "Electrically-assisted evaporation of charged fluids: Fundamental modeling and studies on ionic liquids," Ph.D. thesis, Massachusetts Institute of Technology, 2016.

[21] Boyd, I. D., and Schwartzentruber, T. E., *Nonequilibrium gas dynamics and molecular simulation*, Vol. 42, Cambridge University Press, 2017.